Research Square

Preprints are preliminary reports that have not undergone peer review.
They should not be considered conclusive, used to inform clinical practice,
or referenced by the media as validated information.

Impact of in vitro exposure to 5G-modulated 3.5 GHz fields on human forebrain organoids

Manon Moussay
Université Paris Cité
Delia Arnaud-Cormos
Limoges University, CNRS, XLIM, UMR 7252
Nivetha Sri Pragatheeswaran
Université Paris Cité
Alexandra Albert
Université Paris Cité
Adrien Dufour
Université Paris Cité
Audrey Gibert
Université Paris Cité
Sophie Lebon
Université Paris Cité
Boris Matrot
Université Paris Cité
Pierre Gressens
Université Paris Cité
Sandrine Passemard
Université Paris Cité
Juliette Steenwinckel
Université Paris Cité
Philippe Lévêque
Limoges University, CNRS, XLIM, UMR 7252
Vincent El Ghouzzi
vincent.elghouzzi@inserm.fr

Université Paris Cité

Article

Keywords: 5G-3.5GHz radiofrequency, human forebrain organoid, neurodevelopment

Posted Date: November 13th, 2026

DOI: https://doi.org/10.21203/rs.3.rs-11360170/v1

License: This work is licensed under a Creative Commons Attribution 4.0 International License.
Read Full License

Additional Declarations: No competing interests reported.

Impact of *in vitro* exposure to 5G-modulated 3.5 GHz fields on human forebrain organoids

Manon Moussay[1], Delia Arnaud-Cormos[2,3], Nivetha Sri Pragatheeswaran[1], Alexandra Albert[1], Adrien Dufour[1], Audrey Gibert[1], Sophie Lebon[1], Boris Matrot[1], Pierre Gressens[1], Sandrine Passemard[1,4], Juliette Van Steenwinckel[1], Philippe Lévêque[2], Vincent El Ghouzzi[1]*

[1] Université Paris Cité, Inserm, NeuroDiderot, Paris, France

[2] Limoges University, CNRS, XLIM, UMR 7252, 87000 Limoges, France

[3] France Institut Universitaire de France (IUF), 75005 Paris, France

[4] Service de Neurologie Pédiatrique, DMU INOV-RDB, APHP, Hôpital Robert Debré, Paris, France

*** Correspondence to:**

Vincent El Ghouzzi, Inserm, NeuroDiderot, Paris, France

ORCID ID: 0000-0001-5894-8978

Email : vincent.elghouzzi@inserm.fr

Running title

Key words: 5G-3.5GHz radiofrequency, human forebrain organoid, neurodevelopment

Abstract

The development of 5G mobile technology exposes populations to electromagnetic fields at 3.5 GHz, raising concerns about their effects on human brain development. Most studies on the cerebral effects of radiofrequencies have used rodents, despite major differences between human and rodent corticogenesis, including progenitor subtypes and maturation timing. Here, 40-day-old human forebrain organoids, with actively proliferating apical and basal neural progenitors, were exposed to 5G-modulated 3.5 GHz radiofrequencies at an average specific absorption rate (SAR) of 1.5 W/kg. Effects on neural and glial development were assessed at 7 and 13 weeks using immunocytochemistry and RNA sequencing. Exposed and control organoids showed comparable size and morphology. Progenitor subtype identity and number, proliferation, and apoptotic death rates were similar at both stages. No significant differences were observed in the proportions of cortical neurons, oligodendrocytes, or astrocytes. Transcriptomic analysis confirmed neuronal maturation from 7 to 13 weeks but revealed no significant change in gene expression following exposure.

These findings suggest that, under the in vitro conditions tested, 5G-modulated 3.5 GHz radiofrequencies have no major effect on human forebrain organoid development.

Introduction

The massive increase in wireless technology, which requires ever faster networks capable of feeding multiple connected devices with rich and abundant content, has led to the deployment of the 5G technology, which exploits new frequency bands such as the 3.5 GHz band for very high-speed mobile phone coverage. The number of 5G subscriptions exceeded 2.9 billion in 2025, accounting for more than a third of all mobile subscriptions, and 5G is expected to far outstrip 4G globally within a few years, reaching 6.4 billion subscriptions anticipated by 2031, according to the Ericsson Mobility Report published in November 2025 (https://www.ericsson.com/en/reports-and-papers/mobility-report). In addition to cell phones, all other connected devices are now widely used, with usage times increasing to several hours a day—and even higher among young adults and teenagers. This usage now extends to very young children as well. Finally, fetuses, newborns and infants are passively exposed when they are near an adult using or carrying a transmitting device. Despite this widespread deployment, very few studies are available on the impact of these new frequencies on human health, and in particular, the potential effects of the 5G-associated waves during pregnancy on fetal brain development have not been investigated. Some reports warn of the particular vulnerability of very young children to electromagnetic fields such as the radiofrequencies used in mobile phones [1,2], and a recent randomized study suggests that certain variants may make subpopulations of individuals more vulnerable to 5G-3.6 GHz signals, for example in terms of sleep quality [3]; however, another study aimed at exploring brain electrical activity via EEG in young participants exposed to the same types of signals showed no difference compared to the unexposed group [4]. Consistent with these observations, *in vitro* studies on human skin fibroblasts or keratinocytes exposed to 5G-

modulated 3.5 GHz radiofrequency electromagnetic fields (RF-EMF) showed no evidence of cellular stress or alteration of the DNA repair machinery in the exposed cells [5,6] and SH-SY5Y neuroblastoma cells exposed to 5G-modulated 700 MHz RF-EMF also revealed no biological effects likely to significantly alter mitochondrial reactive oxygen species (ROS) or cell viability [7]. *In vivo*, adult mice subjected to repeated head exposures to 5G-moduated 3.5 GHz signals showed some dysregulation in the expression of genes related to glutamatergic synapses [8]. Although no impact was observed on locomotion, anxiety levels or memory in the exposed mice, the identification of intracortical transcriptional dysregulation - even though it affected less than 1% of expressed genes - suggests that 5G-moduated 3.5 GHz signals may influence cortical development. Here, to investigate this question in a human-derived model, we used 3D guided hiPS-derived forebrain organoids at 7 and 13 weeks of development (50 days and 90 days, respectively) to assess the impact of chronic exposure to 5G-modulated 3.5 GHz signals at a specific absorption rate (SAR) of 1.5 W/kg on human cortical development at the morphological and transcriptional levels. Although *in vitro*, cortical organoids faithfully mimic the early stages of human cortical development, including the formation of neuroepithelial tissue, its apicobasal polarized organization around a lumen that mimics the cerebral ventricle, and the sequential emergence of two major classes of neural progenitors, known respectively as apical progenitors (which divide at the ventricular surface, remain in contact with the ventricle and populate the apical-most germinal zone called the ventricular zone (VZ)), and basal progenitors (which detach from the ventricle and move to a more basal position in the subventricular zone (SVZ)) [9]. Furthermore, human corticogenesis involves two subpopulations of basal progenitors that are very important for human cortical expansion: the so-called intermediate progenitors (IPs), which are also present in mice, and the basal radial glial cells—also known as outer glial cells—which, in contrast, are very few in number in

rodents [10,11]. These different types of progenitor cells are capable of self-amplifying through symmetric proliferative divisions, but also of sequentially generating, through asymmetric neurogenic divisions, the various neurons that will migrate along the radial extensions to position themselves more basally and form the cortical plate. Later in development, the progenitor cells are also capable of generating astrocyte and oligodendroglial populations. Cortical organoids have consequently emerged as powerful human-relevant models for investigating the mechanisms underlying various genetic and environmental brain disorders, ranging from microcephaly and many other neurodevelopmental disorders to virus- or radiation-induced neuropathology or neurodegeneration [12–16]. Their capacity to reproduce human-specific developmental trajectories and cellular responses in a three-dimensional context therefore provides a powerful experimental platform to investigate whether exposure to environmental factors can perturb human cortical development and/or cellular homeostasis. In this study, we utilized the ability of cortical organoids as a model of fetal brain development to replicate the sequential emergence of different cell subpopulations in order to quantify progenitor cells, neurons, astrocytes and oligodendrocytes in the presence and absence of 3.5 GHz signals modulated by 5G, and to assess, via RNA sequencing, the potential effects on gene expression.

Material & Methods

hiPS cell culture and forebrain organoids differentiation

The CtAH hiPS cell line used in this study, generously provided by Pierre Vanderhaeghen's lab (Leuven Brain Institute, Belgium) was selected for its strong neuro-

competence [12,17]. Cells were maintained in 6-well plates in feeder-free conditions on Matrigel (BD/Corning) using StemMACS™ iPS-Brew XF (Miltenyi Biotec) and non-enzymatically dissociated with StemMACS Passaging Solution XF (Miltenyi Biotec). All cells were cultured at 37 °C under 20% O2 and 5% CO2. Forebrain-specific organoids were generated via dual SMAD inhibition of embryoid bodies adapting previously described protocols [18]. Briefly, Embryonic bodies formed from 9,500 hiPS cells were induced in a neural induction medium composed of DMEM/F12 (Life Technologies), 20% KO serum substitute (Life Technologies), 1% MEM-NEAA (Life Technologies), 1% Glutamax (Life Technologies), 1% penicillin-streptomycin (Life Technologies), 2-mercaptoethanol (Sigma), supplemented with bFGF (10 nG/mL, ThermoFisher), Noggin (100 nG/mL, Miltenyi Biotec) and SB-431542 (10 µM, Tocris) for 7 days. On day 7, EBs showing clear optically translucent neuroectoderm were selected and individually transferred to 24-well ultra-low attachment plates in neural medium composed of DMEM/F12 (Life Technologies), N2 supplement (ThermoFisher), 1% MEM-NEAA (Life Technologies), 1% ITS (Life Technologies), 1% penicillin-streptomycin (Life Technologies), supplemented with bFGF (20 nG/mL, ThermoFisher), Noggin (100 nG/mL, Miltenyi Biotec) and SB-431542 (10 µM, Tocris) for 4 days. On day 11, the organoids were embedded in Matrigel drops and cultured without agitation in vitamin A-free differentiation medium composed of DMEM/F12 and Neurobasal (Vol/Vol, Life Technologies), N2 and B27 supplements (ThermoFisher), 1% MEM-NEAA (Life Technologies), insulin (Sigma), 1% Glutamax (Life Technologies), 2-mercaptoethanol (Merck), 1% penicillin-streptomycin (Life Technologies), for an additional 4 days. On day 15, the organoids were transferred to ultra-low attachment Petri dishes in the same medium supplemented with vitamin A with medium renewal twice a week and kept under orbital agitation until their final stage.

Device for organoids exposure to 5G-3.5 GHz signals

Biological samples were exposed to 5G-modulated RF-EMF at 3.5 GHz in a dedicated stainless-steel incubator (Steri-Cycle i160 - ThermoFisher), operating as a reverberation chamber while maintaining physiological culture conditions (37 °C, 5% CO_2) throughout the exposure. A identical incubator was used for the unexposed (control) organoids (**Fig. 1a**). Reverberation chambers generate statistically homogeneous, isotropic, and randomly polarized fields through continuous mechanical stirring, providing highly suitable and controlled exposure conditions for in vitro studies [19,20]. A specific feature of the present exposure setup was the placement of the samples on a Plexiglas support mounted on an orbital shaker (SHEX1619DG, Ohaus), enabling continuous agitation while accommodating up to six Petri dishes.

RF-EMF signals at 3.5 GHz were generated by a vector signal generator (SMBV100A, Rohde & Schwarz) configured to deliver a 5G New Radio (NR, Release 15) waveform employing frequency-division duplexing (FDD), QPSK modulation, and a 100 MHz bandwidth. The signal was amplified using a high-gain power amplifier (ZHL-4W-422+, Mini-Circuits), and subsequently routed through a power circulator (PE83CR1005, Pasternack) and a bidirectional coupler (ZGBDC30-372HP+, Mini-Circuits). Power distribution between the two chambers was controlled via RF switch matrices (RC-1SPDT-18, Mini-Circuits), while incident and reflected powers were continuously monitored using two power meters (U2021A, Keysight). Each chamber incorporated an internal, patch-type antenna and a rotating mechanical stirrer composed of five metallic blades to generate a statistically uniform field environment. Electric field strength was monitored continuously by means of a power detector (ZX47-40-S+, Mini-Circuits) interfaced with a data acquisition unit (34970A, Agilent). Mechanical stirring was

provided by a motorized rotation system consisting of a PRM1/MZ8 rotation stage controlled by a KDC101 DC servo controller (Thorlabs Inc.), both located outside the incubator and operating continuously throughout the exposure period [5,20]. To further improve mode stirring, additional metallic blades were mounted on the orbital shaker, complementing the blades rotating within the incubator volume. Beyond enhancing field uniformity, the continuous orbital shaking also promoted a more homogeneous exposure of the cultured organoids.

Organoids exposure to 5G-3.5 GHz radiofrequencies

30 organoids were generated for each experiment, half of which were cultured in an incubator permanently exposed to radiofrequencies at an average specific absorption rate (SAR) of 1.5 W/kg and the other half in an identical control incubator. In each experiment, 16 organoids were analyzed on day 50 (DIV50) and 14 on day 90 (DIV90), of which 10 were fixed for immunofluorescence analysis and 4-6 were stored for RNA extraction. Each experiment was replicated five times, representing a total of 75 exposed organoids versus 75 control organoids.

Immunofluorescent staining

Three hours prior to fixation, the organoids were incubated in the presence of 5-ethynyl-2'-deoxyuridine (EdU) according to the kit manufacturer's instructions (Pharmingen™ 647 EdU Click Proliferation Kit). After fixation in 4% PFA, the organoids were immersed in a 30% sucrose PBS solution, then embedded in 7.5% gelatin/15% sucrose blocks and cryopreserved before being cryo-sectioned into 20 µm serial sections. For immunocytochemical staining, the sections were first immersed in a PBS solution containing

0.1% Tween, incubated for 60 minutes in a blocking solution containing 0.3% Triton, 6% donkey serum in PBS, and then overnight at 4°C in a solution containing 0.1% Triton, 6% donkey serum in PBS and primary antibodies directed against markers that identify cortical progenitors (SOX2 (abcam ab79351), TBR2 (R&D AF6166), HOPX (Proteintech 11419-1-AP)), neurons (NeuN (Millipore ABN78), HuCD (Invitrogen A21271), CTIP2 (ab18465), CUX1 (ab54583), TBR1 (ab31940)), astrocytes (GFAP (NeuroMics CH22102)), oligodendrocytes (OLIG2 (IBL 18953)), cell proliferation (EdU (Pharmingen 647 EdU Click Proliferation Kit)), KI67 (ab16667) and apoptotic cell death (cleaved CASPASE-3 (Cell Signaling 9661)). After three washes in PBS, the samples were incubated for 60 minutes at room temperature with fluorescent secondary antibodies at a dilution of 1:500 (Jackson Immunoresearch) in the same solution as the previous day, rinsed, incubated in DAPI and mounted with DAKO fluorescence mounting medium. For EdU labelling, the sections were fixed again in 4% PFA right after immunocytochemistry, rinsed and then incubated for 30 min at room temperature in the reagent containing the catalyst, reaction buffer and far-red dye according to the kit manufacturer's instructions, rinsed again and then counterstained with Dapi and mounted with fluorescence medium.

Image analysis and statistics

Immunofluorescent sections were analysed using a Leica TCS SP8 confocal scanning system (Leica Microsystems) except for the mosaics, which were imaged using a Nikon CSU-W1 spinning-disk system. Eight-bit digital images were collected from a single optical plane using a 20x HC PL APO CS2 oil-immersion Leica objective (numerical aperture 0.75) or a 40x HC PL APO CS2 oil-immersion Leica objective (numerical aperture 1.30). For each optical section, double- or triple-fluorescence images were acquired in sequential mode to avoid

potential contamination by linkage specific fluorescence emission cross-talk. Settings for laser intensity, beam expander, pinhole (1 Airy unit), range property of emission window, electronic zoom, gain and offset of photomultiplicator, field format, scanning speed were optimized initially and held constant throughout the study so that all sections were digitized under the same conditions. All images were analysed with Fiji and statistical analysis was performed using GraphPad Prism 8.0 (GraphPad Software, San Diego, CA, USA). Mean values for the experimental groups were calculated and statistically analysed by two-tailed unpaired Student's *t*-test for single comparisons to control. The value of $P < 0.05$ was considered statistically significant. Data are presented as mean $\pm$ SEM. Cell counts were carried out in the areas of interest selected within the VZ/SVZ for progenitor cells and in the cortical plates for neurons and glial cells; the number of labelled cells was expressed as a proportion of the total number of cells (DAPI-positive), excluding cells in mitosis or with pyknotic nuclei.

RNAseq and data analysis

Total mRNAs were extracted using the NucleoSpin RNA Plus kit (Macherey-Nagel®) according to the manufacturer's instructions. cDNA libraries and RNA sequencing Library preparation and Illumina sequencing were performed at the Ecole Normale Supérieure GenomiqueENS core facility (Paris, France). mRNA sequencing libraries were prepared using the Illumina Stranded mRNA Ligation library preparation protocol (Illumina, San Diego, CA, USA), according to the manufacturer's instructions. Libraries were multiplexed by 16 on P3 flow cells. A 68 bp read sequencing was performed on a NextSeq 2000 device (Illumina). A mean of 35 ± 10 million passing Illumina quality filter reads was obtained for each of the 16 samples. The analyses were performed using the Eoulsan pipeline [21] including read filtering, mapping, alignment filtering, read quantification using Human GRCh38 ENsembl 105

reference genome. Normalization of sample counts, statistical treatments, and differential analyses were performed using DESeq2 1.8.1 [22]. Differentially expressed transcripts between time points or between experimental conditions were identified after filtering on a BH-adjusted p-value < 0.05. Functional annotations in the figures were obtained using Metascape tool v3.5 (http://metascape.org). PPI networks were built using STRING 12.0 (https://string-db.org).

Results

Device settings and induction protocol

The setup for exposure to an SAR of 1.5 W/kg was installed in a dedicated incubator serving as a reverberation chamber, as described in the Methods section, and an identical incubator was used for the non-exposed conditions (**Fig. 1a**). The organoids were distributed between the two chambers according to a blind experimental protocol in accordance with established laboratory practices for studies on the biological effects of radiofrequency electromagnetic fields [23]. Exposure characterization relied on a combination of numerical and experimental dosimetry, by following a methodology that we have previously described [7,24]. An average SAR of 2.0 ± 0.2 W/kg per watt of incident power was obtained within the Petri dishes containing the organoids. Based on these results, the input power was set to deliver a target average SAR of 1.5 W/kg during the 5G-modulated 3.5 GHz exposures.

Forebrain organoids were generated from embryoid bodies induced by DUAL SMAD inhibition for 7 days, then embedded in Matrigel droplets on day 11 and placed in an orbital shaker starting on day 15, following the steps initially described by Lancaster and adapted for guided neuroepithelial differentiation [18]; (**Fig. 1b**) (also see Methods). Chronic exposure to

5G-modulated 3.5 GHz radiofrequencies began on day 40, and samples were analyzed on day 50 (DIV50, 10-day exposure) —a stage at which both apical and basal progenitor cells are actively proliferating—and on day 90 (DIV90, 50-day exposure), a stage at which not only neurons but also oligodendrocytes and astrocytes are present. To reduce sample-related heterogeneity in downstream analyses, the organoids used for immunohistochemical analyses and those used for transcriptomic analysis were derived from the same batches.

Organoid size and overall morphology upon RF chronic exposure

As they grew and with each change of medium, the organoids were observed macroscopically from day 40 up to day 90. As expected, control organoids exhibited a well-defined spherical morphology and high refractility, reaching a mean diameter of 3 mm by day 70. No notable differences in size or overall morphology were observed between the control group and the exposed group (**Fig. 2a**). On DIV50 and DIV90, the organoids were fixed, embedded, sectioned and immunostained for progenitors (SOX2, TBR2, HOPX) and neuronal markers (TBR1, CTIP2). Analysis of sections from whole organoids enabled us to measure the average surface area of the samples at both stages of differentiation (**Fig. 2b**). The average surface area of the sections was 2.5 mm^2 on day 50 and reached 4.7 mm^2 on DIV90, with no significant difference between the control group and the exposed group, confirming our initial observation (**Fig. 2c**). Furthermore, a large number of structures in the organoids from both groups exhibited a well-defined neuroepithelial organization, with a VZ populated by SOX2-expressing progenitors polarized around a ventricle, a SVZ containing intermediate progenitors (TBR2) and basal radial glial cells (HOPX) and a cortical plate located more basally. These results suggest that chronic exposure of the organoids does not affect the overall growth of the neuroepithelium.

Impact of chronic exposure on cortical progenitor cell proliferation, differentiation and apoptosis

We then examined in greater detail the identity and number of neural progenitors generated in the VZ and SVZ on DIV50 and DIV90. Because the size of VZs varies considerably from one neuroepithelial structure to another within the same organoid, we quantified the number of SOX2+, TBR2+ or HOPX+ progenitor cells relative to the total number of cells (DAPI) in each neuroepithelial region considered. Cells that were positive for SOX2 but negative for TBR2 and HOPX were considered to be apical progenitors, whilst cells positive for TBR2 were identified as intermediate basal progenitors and those positive for HOPX were identified as basal radial glial cells. However, none of the markers showed any statistically significant differences between the control group and the exposed group, either on day 50 or on day 90 (**Fig. 3a–b**), indicating that chronic radiofrequency exposure has no effect on the number of neural progenitors in the condition tested. To confirm this observation, we quantified the number of proliferating progenitor cells using the cell cycle marker Ki67, and we also quantified the incorporation of EdU, a thymidine analogue that is incorporated into DNA during replication and reflects the proliferative potential of progenitor cells. We detected no difference in the proliferative potential of the progenitor cells between the two groups and at the two stages analyzed (**Fig. 3a–b**), confirming that radiofrequency exposure had no significant impact on the progenitor cell proliferation in our *in vitro* forebrain organoids. To test whether chronic exposure to radiofrequency radiation could affect the survival of progenitor cells or neurons, we then performed immunolabelling on the organoids at DIV90 using the apoptotic marker cleaved caspase-3. The majority of caspase labelling was confined to the VZ, with very few neurons being labelled. Neuronal density, assessed using the neuronal

marker HUCD, was similar between the two groups. Quantification of the apoptotic signal in the VZ revealed no significant difference between the control group and the exposed group (**Fig. 3b**). These data indicate that chronic exposure of forebrain organoids to 5G-modulated 3.5 GHz radiofrequencies does not impair neural progenitor cell proliferation, differentiation or survival.

Impact of chronic exposure on cortical neuron maturation and glial cells

We then assessed the ability of the organoids to generate the various subpopulations of cortical neurons, as well as glial cells derived from the same progenitors within the cortical pre-plate on day 50 and day 90. The pan-neuronal markers MAP2, NeuN, and TUJ1 were used to label neurons regardless of their stage of maturation (TUJ1) or the dendrites (MAP2) and nuclei (NeuN) of mature neurons. Both the control organoids and the exposed organoids were able to generate immature and mature neurons, with an increase in the cortical plate formation on DIV90 compared to DIV50 in both groups. Quantification of the nuclear marker NeuN showed no statistically significant difference between the two groups, regardless of the stage analyzed (**Fig. 4a-b**). Similarly, analysis of the nuclear markers CTIP2, TBR1, and CUX1—which identify subpopulations of cortical neurons—showed no quantitative difference between the two groups, indicating that chronic exposure to radiofrequencies does not affect the differentiation of cortical neurons. Finally, to quantify glial cells, we analyzed the OLIG2 marker, which is specifically expressed in oligodendrocytes regardless of their stage of maturation, and the GFAP marker, which reflects the astrocyte population. OLIG2 was already detectable by day 50 in the majority of neuroepithelial structures but was largely confined to the VZ at this stage, whereas by day 90, oligodendrocytes were preferentially present in the more basal regions. However, no significant differences were observed between the two

groups at either stage for OLIG2 staining (**Fig. 4a-b**). GFAP was not present on day 50 but only on day 90, indicating a later appearance of astrocytes in forebrain organoids. However, the signal quantification again showed no significant difference between the control group and the exposed group at DIV90 (**Fig. 4b**). Taken together, these data indicate that chronic exposure to 5G-modulated 3.5 GHz radiofrequencies does not significantly affect the maturation of cortical neurons and glial cells in forebrain organoids.

Transcriptomic analysis of forebrain organoids upon RF exposure

We next investigated the transcriptomic effects of radiofrequency exposure in human forebrain organoids at both DIV50 and DIV90. We first characterized the transcriptional changes associated with the *in vitro* development of control organoids by comparing transcriptomic profiles between DIV50 and DIV90, thereby identifying the molecular processes underlying human forebrain organoid maturation. Differential expression analysis between DIV50 and DIV90 identified 346 differentially expressed genes (DEGs; padj < 0.05, |L2FC| > 0.25), visualized on a volcano plot (**Fig.5a, Supp Table 1**). Among down-regulated genes, *PAX6* and *IGF2BP1* mRNA, both neural progenitor markers, were highlighted, consistent with progressive neuronal maturation between DIV50 and DIV90.

Functional annotation using Gene Ontology, Hallmark and Reactome databases of up-regulated DEGs (**Fig.5b, Supp Table 2**) identified significant enrichment (p-value < 0.01, a minimum count of 3, and an enrichment factor > 1.5) for lipid metabolism (acylglycerol homeostasis), vascular processes (including regulation of nitric oxide biosynthesis, response to hypoxia, positive regulation of VEGF production), synaptic function (trans-synaptic signaling modulating synaptic transmission, memory), negative regulation of cell proliferation and growth, monocarboxylic acid transport, interferon alpha response, and regulation of hormone

levels. A complementary analysis of the down-regulated gene set (**Fig.5b, Supp Table 3**) identified cholesterol biosynthesis, the G2M checkpoint, glycosaminoglycan (heparan sulfate/heparin) biosynthesis, sensory organ development, and cell-cell signaling as additional pathways down-regulated processes induced by organoid development.

Protein-protein interaction (PPI) network analysis of down-regulated DEGs (**Fig.5c, Supp Table 4**) demonstrated significant network enrichment (PPI enrichment p=0.000145, confidence 0,5) and revealed three major modules containing at least three nodes: a cell-cycle-associated module (CCNA2, CCND1, CKS1B, PTTG1, HMMR, LIN52), a cholesterol/sterol biosynthesis module (DHCR24, FDPS, LSS, ACAT2), transcription factor-associated module (SOX3, PAX6, CRYGD). The PPI network built from up-regulated DEGs (**Fig.5c, Supp. Table 5**) (PPI enrichment $p = 9.03 \times 10^{-5}$, confidence 0.5) was markedly larger and interconnected, centered around APOE and GFAP, both markers of astrocyte/glial maturation. This network extended to circadian and WNT signaling components (RORA, PER3, ITPR1, WNT9A, WNT10B, SFRP4), interferon-response genes (IFIT2, IRF9), extracellular matrix/collagen-related genes (COL8A2, COLGALT2, PLA2G4B), and a gap junction-associated cluster (GJB2, GJB6). Together, these findings reflect broad transcriptional remodeling and maturation during organoid development.

We next investigated the transcriptomic impact of radiofrequency exposure in human forebrain organoids at DIV50 and DIV90. Principal component analysis (PCA) (**Fig.5d**) revealed that samples clustered according to developmental stage, with PC1 explaining 48% of the total variance. In contrast, control and exposed samples largely overlapped within each developmental stage, and PC2, which accounted for 19% of the variance, did not distinguish exposed from control organoids. These findings indicate that radiofrequency exposure does not induce a detectable global transcriptional signature. Differential expression analysis

between exposed and control organoids showed no significant DEGs at either DIV50 or DIV90, indicating that radiofrequency exposure had no detectable effect on the organoid transcriptome at either developmental stage (**Supp. Table 6).** PAX6 mRNA normalized count significantly decreased between DIV50 and DIV90, consistent with the expected transition from an early neural progenitor state toward more differentiated cell population during development. Importantly, this developmental down-regulation of PAX6 expression was not altered in RF-exposed organoids, suggesting that RF exposure did not interfere with the regulation of this key neurodevelopmental transcription factor.

Discussion

The developing brain is particularly vulnerable to environmental insults, owing to the highly dynamic and tightly regulated processes underlying neurogenesis, neuronal and glial differentiation and maturation. Urban environments, in particular, present a specific set of environmental stressors, such as traffic-related air pollution or noise, which can affect mental health in adults but have also been linked to neurodevelopmental defects [25–27]. However, the impact of electromagnetic waves from 5G mobile communication technology—which has seen tremendous growth in recent years—on brain development has been studied very little to date in human-derived models. Here, we evaluated the effects of chronic exposure to 5G-modulated 3.5 GHz radiofrequencies on the development of 7- and 13-week-old forebrain organoids derived from human induced pluripotent stem cells. At both stages examined, neither neural progenitors, cortical neurons, nor glial cells appeared to be affected by radiofrequency exposure. These observations were confirmed by similar proliferation and apoptosis levels in the control and exposed groups, as well as by transcriptomic analyses at 7

and 13 weeks of development, which revealed no dysregulated genes or pathways in the exposed group. Our study therefore found no significant adverse effects on early brain development due to chronic exposure to radiofrequency radiation under the conditions used. Our findings are consistent with several other *in vitro* studies, although those studies used different human cell types and involved different exposure protocols: In a study evaluating the environmental cell stress response of immortalized human skin fibroblasts and keratinocytes, continuous or intermittent (5 min ON followed by 10 min OFF) exposure to 5G-modulated 3.5 GHz radiofrequencies at SAR levels between 0.25 and 4 W/kg for 24 hours revealed no significant molecular effects on HSF1, RAS/ERK, and PML proteins—used as proxies for environmental stresses such as thermal injury, oxidative stress, and proteotoxic stress [6]. In a similar model using immortalized fibroblasts and with comparable exposure for 24 hours, Haidar et al. concluded that exposure to 5G radiofrequencies at 3.5 GHz up to 4 W/kg does not induce oxidative stress or impair DNA repair efficiency in human skin cells [5]. Two studies using human SH-SY5Y neuroblastoma cells also found no adverse effects on the cell cycle or DNA damage [28] or on the production of ROS, cell viability, and apoptosis [7] at SAR values ranging from 1 to 4 W/kg, and using the 26.5 GHz and 700 MHz frequency bands respectively.

Although the exposure times to 5G radio waves differed between these studies and ours, the specific absorption rates used were within a range comparable to the one we applied to the organoids in our study (1.5 W/kg). Thus, under conditions consistent with environmental standards, 5G-modulated 3.5 GHz radiofrequencies do not appear to have a deleterious effect on these different cell types. Our study further shows that the polarized three-dimensional organization of the neuroepithelium is not affected and that the cortical plate, cortical neurons, astrocytes, and oligodendrocytes form at the same developmental stage and in the

same proportions in both groups. Furthermore, our model shows that even prolonged exposure lasting between 10 and 50 days does not cause any harmful effects on the neuroepithelium. Although these exposures are much longer than those tested in the cellular models cited below, they remain well below the actual duration for which a human brain is exposed in an urban environment throughout its development. Forebrain organoids at 7 and 13 weeks would indeed correspond to first- and second-trimester human fetal brain, respectively, according to the transcriptomic similarities identified in comparison with *in vivo* fetal cortex [16,29,30]. It would therefore be important to reassess the effect of 5G radiofrequencies using organoid models that are older than those used in this study, thereby targeting a stage of development at which neuronal and glial cells have reached a more advanced stage of maturation, forming functional networks, and might respond differently to their environment [29,31,32]. Re-evaluating the effect of radiofrequencies on organoids that also contain vascularization and microglia would undoubtedly also enable their impact to be assessed under conditions that are physiologically closer to *in vivo* tissue. This would also allow the evaluation of potential synergistic effects, for example by mimicking a proinflammatory environment. In a study involving developing rats subjected to LPS-induced pro-inflammatory stress, a single head exposure to GSM-1800 MHz at a SAR of 2.9 W/kg was shown to be sufficient to modulate pro-inflammatory genes and microglial cell responses in the cortex [33]. Although these experiments have not been replicated in a 5G context, they suggest that electromagnetic fields could modulate cellular responses triggered by a pre-existing pro-inflammatory background. It is interesting to note that the same authors recently evaluated the effects of 5G-modulated 3.5 GHz signals on gene expression in the cortex of adult mice, this time using chronic exposure of one hour per day, 5 days a week, over a 6-week period, and demonstrated changes in the expression of a limited set of genes that could affect

glutamatergic synapses and mitochondrial activity [8]. Although no effects were observed on locomotion, anxiety levels, or memory capacity in these mice, these changes in gene expression following prolonged chronic exposure—even though they involved less than 1% of the expressed genes—clearly demonstrate that the experimental background is essential for drawing reliable conclusions.

Ultimately, our study on organoids reaches the reassuring conclusion that chronic exposure to 5G-modulated 3.5 GHz radiofrequency radiation has no significant impact on the morphology, development, and gene expression of the human cortical neuroepithelium under the conditions tested; however, it calls for further investigation to confirm these observations in even more mature and physiologically-relevant models.

References

1. Moon, J.-H. Health effects of electromagnetic fields on children. *Clin Exp Pediatr* **63**, 422–428 (2020).
2. Stewart, W. *Mobile Phones and Health, Report of Independent Expert Group on Mobile Phones*. https://webarchive.nationalarchives.gov.uk/ukgwa/20101007133914/http://www.iegmp.org.uk/report/index.htm (2000).
3. Sousouri, G. *et al.* 5G radio-frequency-electromagnetic-field effects on the human sleep electroencephalogram: A randomized controlled study in CACNA1C genotyped volunteers. *Neuroimage* **317**, 121340 (2025).
4. Jamal, L. *et al.* Assessment of Electrical Brain Activity of Healthy Volunteers Exposed to 3.5 GHz of 5G Signals within Environmental Levels: A Controlled-Randomised Study. *Int J Environ Res Public Health* **20**, 6793 (2023).
5. Haidar, J. *et al.* Impact of in vitro exposure to 5G-modulated 3.5 GHz fields on oxidative stress and DNA repair in skin cells. *Sci Rep* **15**, 31214 (2025).
6. Joushomme, A. *et al.* Effects of 5G-modulated 3.5 GHz radiofrequency field exposures on HSF1, RAS, ERK, and PML activation in live fibroblasts and keratinocytes cells. *Sci Rep* **13**, 8305 (2023).
7. Puginier, E. *et al.* Biological effects of 5G-modulated 700 MHz RF-EMF exposure on neuronal and glial cell models under isothermal conditions. *Sci Rep* **16**, 10767 (2026).

8. Lameth, J. *et al.* Repeated Head Exposures to a 5G-3.5 GHz Signal Do Not Alter Behavior but Modify Intracortical Gene Expression in Adult Male Mice. *Int J Mol Sci* **26**, 2459 (2025).
9. Taverna, E., Gotz, M. & Huttner, W. B. The cell biology of neurogenesis: toward an understanding of the development and evolution of the neocortex. *Annu Rev Cell Dev Biol* **30**, 465–502 (2014).
10. Namba, T. & Huttner, W. B. Neural progenitor cells and their role in the development and evolutionary expansion of the neocortex. *Wiley Interdiscip Rev Dev Biol* **6**, (2017).
11. Pinson, A. & Huttner, W. B. Neocortex expansion in development and evolution-from genes to progenitor cell biology. *Curr Opin Cell Biol* **73**, 9–18 (2021).
12. Albert, A. *et al.* Oropouche virus infects human neural progenitor cells and alters the growth of brain organoids. *iScience* **29**, 114957 (2026).
13. Birtele, M., Lancaster, M. & Quadrato, G. Modelling human brain development and disease with organoids. *Nat Rev Mol Cell Biol* **26**, 389–412 (2025).
14. Farcy, S., Albert, A., Gressens, P., Baffet, A. D. & El Ghouzzi, V. Cortical Organoids to Model Microcephaly. *Cells* **11**, 2135 (2022).
15. Lancaster, M. A. *et al.* Cerebral organoids model human brain development and microcephaly. *Nature* **501**, 373–9 (2013).
16. Velasco, S. *et al.* Individual brain organoids reproducibly form cell diversity of the human cerebral cortex. *Nature* **570**, 523–527 (2019).
17. Espuny-Camacho, I. *et al.* Pyramidal neurons derived from human pluripotent stem cells integrate efficiently into mouse brain circuits in vivo. *Neuron* **77**, 440–56 (2013).
18. Lancaster, M. A. & Knoblich, J. A. Generation of cerebral organoids from human pluripotent stem cells. *Nat Protoc* **9**, 2329–2340 (2014).

19. Zeni, O. *et al.* Formation of reactive oxygen species in L929 cells after exposure to 900 MHz RF radiation with and without co-exposure to 3-chloro-4-(dichloromethyl)-5-hydroxy-2(5H)-furanone. *Radiat Res* **167**, 306–311 (2007).
20. Christ, A., Klingenbock, A., Samaras, T., Goiceanu, C. & Kuster, N. The dependence of electromagnetic far-field absorption on body tissue composition in the frequency range from 300 MHz to 6 GHz. *IEEE Trans. Microwave Theory Techn.* **54**, 2188–2195 (2006).
21. Jourdren, L., Bernard, M., Dillies, M.-A. & Le Crom, S. Eoulsan: a cloud computing-based framework facilitating high throughput sequencing analyses. *Bioinformatics* **28**, 1542–1543 (2012).
22. Love, M. I., Huber, W. & Anders, S. Moderated estimation of fold change and dispersion for RNA-seq data with DESeq2. *Genome Biol* **15**, 550 (2014).
23. Kuster, N. & Schönborn, F. Recommended minimal requirements and development guidelines for exposure setups of bio-experiments addressing the health risk concern of wireless communications. *Bioelectromagnetics* **21**, 508–514 (2000).
24. Orlacchio, R. *et al.* A Novel Reverberation Chamber for In Vitro Bioelectromagnetic Experiments at 3.5 GHz. *IEEE Trans. Electromagn. Compat.* **65**, 39–50 (2023).
25. Morrel, J. *et al.* A systematic review of air pollution exposure and brain structure and function during development. *Environ Res* **275**, 121368 (2025).
26. Bilinovich, S. M. *et al.* Integrated RNA Sequencing Reveals Epigenetic Impacts of Diesel Particulate Matter Exposure in Human Cerebral Organoids. *Dev Neurosci* **42**, 195–207 (2020).
27. Hahad, O. *et al.* Cerebral consequences of environmental noise exposure. *Environ Int* **165**, 107306 (2022).

28. Sannino, A. *et al.* Exposure to 26.5 GHz, 5G modulated and unmodulated signal, does not affect key cellular endpoints of human neuroblastoma cells. *Sci Rep* **15**, 20614 (2025).
29. Faravelli, I., Antón-Bolaños, N., Wei, A. et al. Human brain organoids record the passage of time over multiple years. *Nature* (2026) doi:10.1038/s41586-026-10877-x.
30. Pollen, A. A. *et al.* Establishing Cerebral Organoids as Models of Human-Specific Brain Evolution. *Cell* **176**, 743-756.e17 (2019).
31. Giandomenico, S. L., Sutcliffe, M. & Lancaster, M. A. Generation and long-term culture of advanced cerebral organoids for studying later stages of neural development. *Nat Protoc* **16**, 579–602 (2021).
32. Petersilie, L. *et al.* Protocol for the generation of cultured cortical brain organoid slices. *STAR Protoc* **5**, 103212 (2024).
33. Lameth, J. *et al.* Acute Neuroinflammation Promotes Cell Responses to 1800 MHz GSM Electromagnetic Fields in the Rat Cerebral Cortex. *Neurotox Res* **32**, 444–459 (2017).

Acknowledgements and Funding

We would like to thank the National Health Security Agency (ANSES) for funding this study (ANSES-21-RF-24) to V.E.G and P.L – The French National Research Program for Environmental and Occupational Health of Anses, with the support of the ministries responsible for the environment, agriculture and labor, and the Paris Brain Child Institute (ICE) for its support of the NeuroDiderot Human Brain Organoid core facility (HumBO), as part of the France 2030 program (ANR-23-IAHU-0010). We are also grateful to Cécile Martel for invaluable support. NeuroDiderot is affiliated to C-BRAINS, a field of major innovation and research (DIM) supported by the Ile-de-France Regional Council.

Competing interests

The authors declare no competing interest.

Author contributions

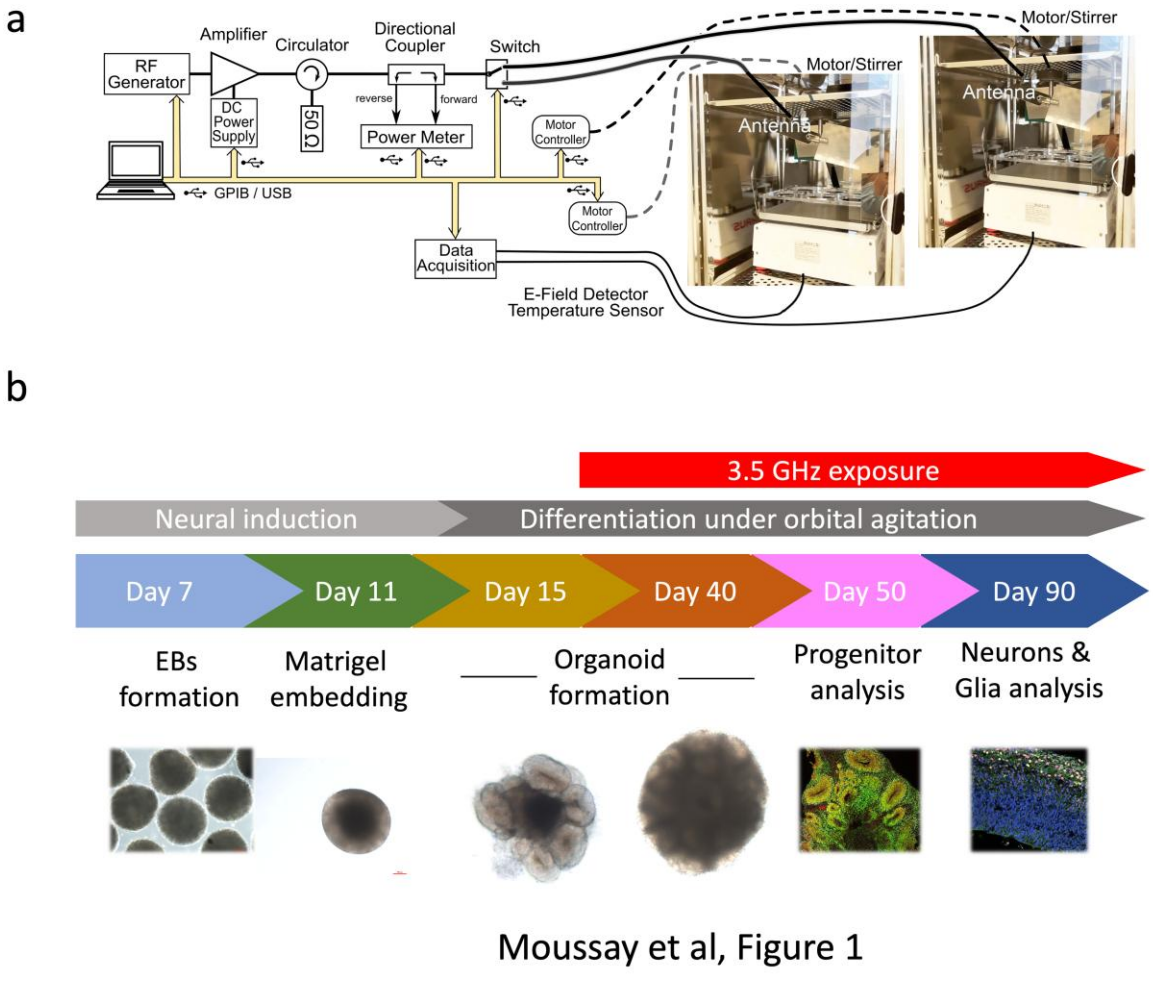
Conceptualization, V.E.G., P.L. and B.M.; V.E.G supervised the project; P.L. and D.A. designed the 5G exposure device and settings; M.M., N.S.P. generated and grew the cerebral organoids with the help of with the help of A.A. and V.E.G.; M.M, S.L. and A.A prepared the organoid samples for slicing or RNA extraction; M.M. and N.S.P. performed the immunostaining and analyzed the images with the help of S.P; A.D., A.G. and J.V.S. performed RNAseq and transcriptomic analyses; V.E.G. wrote the manuscript with the inputs from P.L., J.V.S. and D.A.; Funding Acquisition, V.E.G., P.L., B.M. and P.G.

Figure legends

Figure 1. Exposure device and procedure for the differentiation and culturing of Human Forebrain Organoids.

(a) Device for exposing organoids to 5G-3.5 GHz signals: a diagram of the experimental setup, showing the multi-component unit positioned outside the incubators, and a photograph of the control device installed inside each incubator.

(b) Schematic representation of human forebrain organoid generation and timeline of exposure to 3.5 GHz electromagnetic fields.



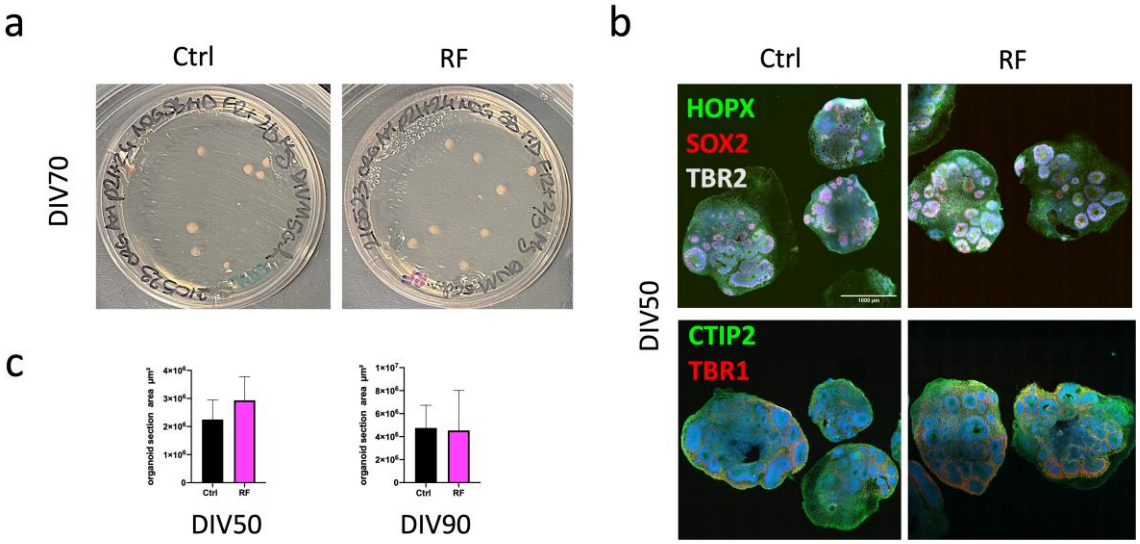
Moussay et al, Figure 1

Figure 2. Morphology and structure of control (Ctrl) and exposed (RF) whole forebrain organoids

(a) Macroscopic appearance of the organoids on day 70.

(b) Morphology of (Ctrl) and exposed (RF) whole organoids on day 50 and day 90 following immunohistochemistry identifying the progenitor regions (SOX2, TBR2, HOPX) and the more basal, differentiated regions (TBR1, CTIP2). Scale bar = 1 mm

(c) Quantification of the average surface area of control (Ctrl) and exposed (RF) whole organoid sections on day 50 and day 90. Data are presented as mean ± SEM. *P≤0.05 (Student's t-test).



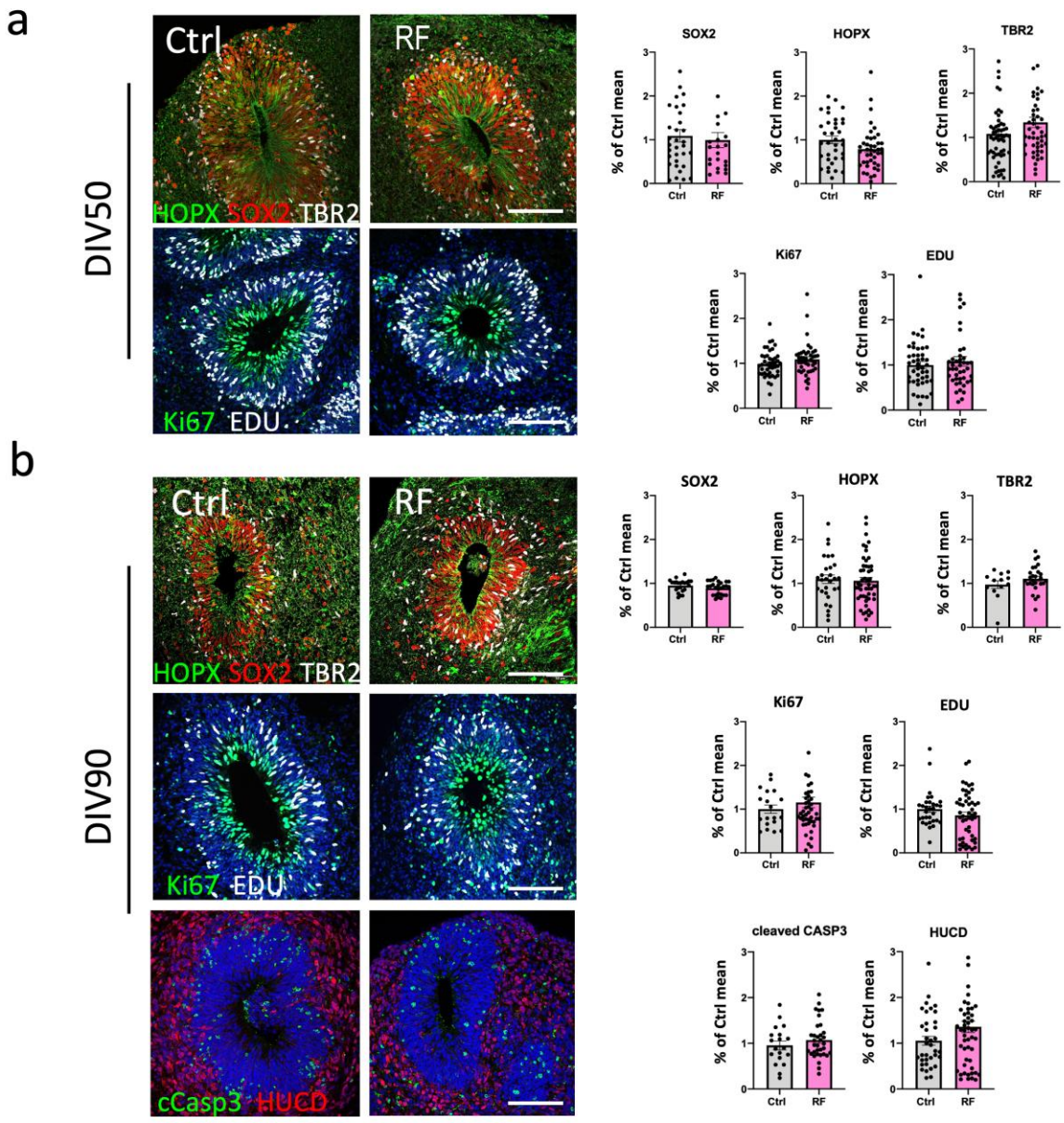
Moussay et al, Figure 2

Figure 3. Immunohistochemical analysis of cortical progenitors on day 50 and day 90

(a) Immunofluorescent staining and representative quantification of the ventricular zone of control (Ctrl) or exposed (RF) organoids showing progenitors at day 50 labelled with SOX2 (red), TBR2 (white), HOPX (green) or showing the proportion of cells that incorporated EdU

for 3 hours prior to fixation (in white), cells in cycle (Ki67+ in green) and DAPI (blue). Quantifications are expressed as a percentage of the mean value for the control group ± SEM. *P≤0.05 (Student's t-test). Scale bar = 100 μm.

(b) Immunofluorescent staining and representative quantification of the ventricular zone of control (Ctrl) or exposed (RF) organoids showing progenitors at day 90 labelled with SOX2 (red), TBR2 (white), HOPX (green) (top images), the proportion of cells that incorporated EdU for 3 hours prior to fixation (in white), cells in cycle (Ki67+ in green) and DAPI (blue) (centre images), the cleaved caspase 3 fluorescent signal (green) and neuron stained with HUCD (red) and DAPI (blue) (bottom images). Quantifications are expressed as a percentage of the mean value for the control group ± SEM. *P≤0.05 (Student's t-test). Scale bar = 100 μm.



Moussay et al, Figure 3

Figure 4. Immunohistochemical analysis of cortical neurons and glial cells on day 50 and day 90

Immunofluorescent staining and representative quantification of cortical neurons and glial cells in control (Ctrl) and exposed (RF) organoids at day 50 **(a)** and day 90 **(b)** labelled with TUJ1 (red), MAP2 (white), NeuN (green) and DAPI (blue) (top images), TBR1 (red), CTIP2 (green) or CUX1 (red) and DAPI (blue) (centre images), OLIG2 (green), GFAP (white) and DAPI

(blue) (bottom images). Quantifications are expressed as a percentage of the mean value for the control group ± SEM. *P≤0.05 (Student's t-test). Scale bar = 100 µm.

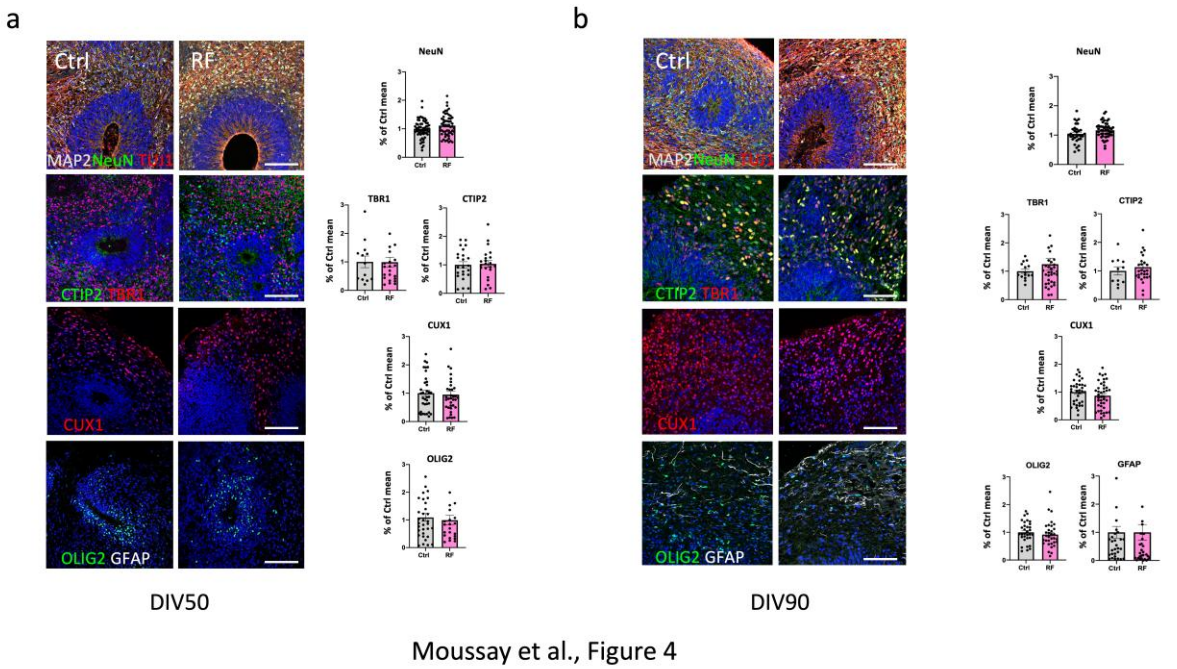
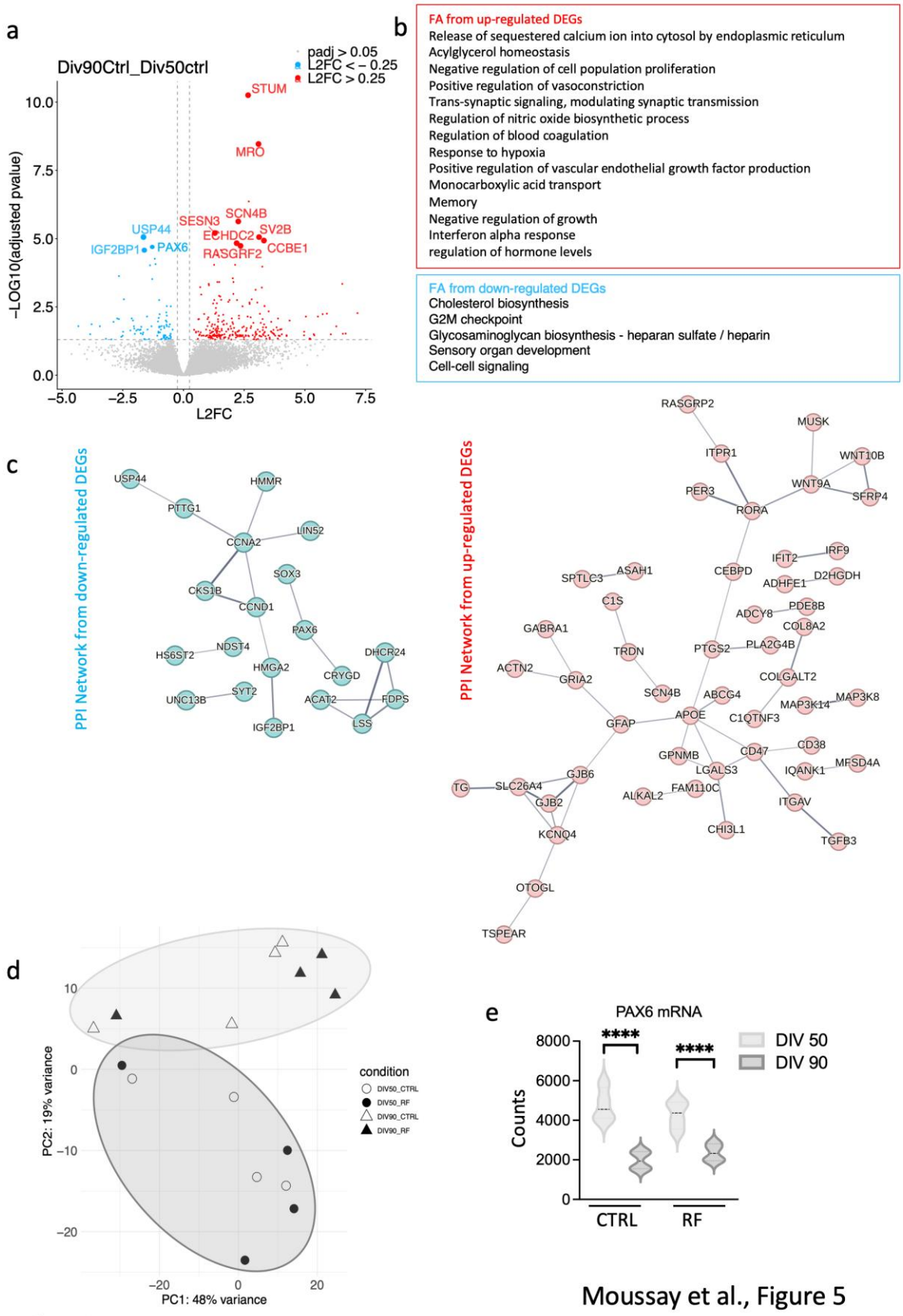


Figure 5. Transcriptomic analysis of organoids at DIV50 and DIV90 and following RF exposure.

(a) Volcano plot showing differential gene expression between DIV50 and DIV90 organoids in control condition (adjusted *p*-value < 0.05 and |log2 fold change (L2FC)| > 0.25). **(b)** Functional enrichment analysis of up- and down-regulated DEGs using Gene Ontology, Hallmark, and Reactome databases identified significantly enriched terms. **(c)** Protein-protein interaction (PPI) network analysis of the up- and down-regulated DEGs. **(d)** Principal component analysis (PCA) of transcriptomic profiles from DIV50 and DIV90 organoids exposed or not exposed to radiofrequency (RF) radiation. **(e)** *PAX6* mRNA expression in DIV50 and DIV90 organoids exposed or not exposed to RF radiation.



Moussay et al., Figure 5

Supplementary Table Legends

Supplementary Table 1. Differential gene expression at DIV90 versus DIV50 under control conditions.

Supplementary Table 2. Functional analysis of genes significantly upregulated at DIV90 versus DIV50 under control conditions.

Supplementary Table 3. Functional analysis of genes significantly downregulated at DIV90 versus DIV50 under control conditions.

Supplementary Table 4. Node degrees and network coordinates in the protein-protein interaction (PPI) network constructed from differentially expressed genes (DEGs) up-regulated at DIV90 versus DIV50 under control conditions.

Supplementary Table 5. Node degrees and network coordinates in the protein-protein interaction (PPI) network constructed from differentially expressed genes (DEGs) down-regulated at DIV90 versus DIV50 under control conditions.

Supplementary Table 6. Differential gene expression between RF and control conditions at DIV50 and DIV90.

Supplementary Files

This is a list of supplementary files associated with this preprint. Click to download.

- MoussayetalSuppTable1.xlsx
- MoussayetalSuppTable2FAUP.xlsx
- MoussayetalSuppTable3FADOWN.xlsx
- MoussayetalSuppTable4.xlsx
- MoussayetalSuppTable5.xlsx
- MoussayetalSuppTable6.xlsx